ADVANCED ELECTRONIC MATERIALS
www.advelectronicmat.de

Synergistic Photomodulation of Capacitive Coupling and Charge Separation Toward Functional Organic Field-Effect Transistors with High Responsivity

*Hongtao Zhang, Jingshu Hui, Hongliang Chen, Jianming Chen, Wei Xu, Zhigang Shuai, Daoben Zhu, and Xuefeng Guo**

Organic field-effect transistors (OFETs) are the basic building blocks in numerous flexible integrated circuits and displays; over the past 25 years, significant advances have been made with respect to OFETs by improving the performance of organic semiconductors as well as modulating the engineering of devices.[1] Of note, a very high carrier mobility of >8 $cm^2 V^{-1} s^{-1}$ has been reported for both conjugated polymers and small-molecule organic semiconductors,[2] which warrants the practical commercialization of OFETs. Meanwhile, novel OFETs with specific functions, such as non-volatile memory devices,[3] phototransistors,[4] light-emitting transistors,[5] and OFET-based chemical or biosensors,[6] have been demonstrated, thereby providing a promising direction for organic electronics.[3c,7] In view of this direction, for building functional organic electronic devices, a particularly urgent requirement is to develop efficient strategies to control the carrier density in the conductive channel of OFETs.

Apart from the development of high-mobility organic semiconductors, functional high-performance OFETs can be effectively built by interface engineering because the nature of the interfaces that are ubiquitous in OFETs plays an important role in the performance and stability of devices.[8] Among different interfaces, the dielectric/semiconductor interface is particularly vital as, under an applied electric field, charge carriers are directly generated and transported at this interface. Hence, the polarity, charge distribution, and surface roughness of the dielectric/semiconductor interface can dramatically affect the device performance. Besides these factors, intrinsic characteristics of dielectric materials, such as permittivity, can also influence the carrier transport in the semiconductor. Therefore, it is essential to modify the dielectric/semiconductor interface and functionalize dielectric layers for providing straightforward methods to tailor the carrier density and/or install new functions.[9] In this study, we demonstrate such a general approach to fabricate a new type of organic phototransistor, which is capable of reversibly photomodulating the carrier density at the dielectric/semiconductor interface; this phototransistor was constructed using photochromic spiropyran (SP)–methyl methacrylate (MMA) copolymers (hereafter referred to as SP-*co*-MMA) as the photoresponsive gate dielectrics (**Figure 1**). SP is a type of organic chemical compounds known for its photochromic properties;[10] it was chosen as the photosensitizer because SPs can revert back-and-forth between a neutral, closed form (SP-closed) and a zwitterionic, open form (SP-open) when exposed to light of different wavelengths. Such a unique conformational transition caused by the photoisomerization of SP molecules leads to a significant modulation of the electric dipole moment (P_{mol}) (≈6.4 D of SP-closed and ≈13.9 D of SP-open),[11] thus forming the basis of the development of novel photoswitchable sensors and functional optoelectronic devices.[12] In this case, reversible P_{mol} changes of SPs in polymer dielectrics result in two distinct capacitance values that induce different capacitive coupling. In addition, under UV irradiation, SPs at the dielectric/semiconductor interface could change from a neutral form (SP-closed) to a charge-separated form (SP-open), thus producing scattering sites that can trap the photoexcited electrons and correspondingly leave hole carriers in the conductive channel. A synergistic combination of both effects realizes the photomodulation of the threshold voltage (V_T) values, and thus channel conductance. This study is established from previous cases where SP was simply mixed with poly(methyl methacrylate) (PMMA) as the gate dielectric; unfortunately, the SP concentration was significantly limited by its low solubility in PMMA.[9d,f] The important distinction in this study is that the use of SP-*co*-MMA copolymers allows for the substantial tuning of the SP ratios in polymer dielectrics, thus significantly

Dr. H. Zhang,[+] J. Hui, H. Chen, Prof. X. Guo
Center for Nanochemistry
Beijing National Laboratory for Molecular Sciences
State Key Laboratory for Structural Chemistry of Unstable and Stable Species
College of Chemistry and Molecular Engineering
Peking University
Beijing 100871, P. R. China
E-mail: guoxf@pku.edu.cn
Dr. J. Chen, Prof. W. Xu, Prof. D. Zhu
Key Laboratory of Organic Solids
Beijing National Laboratory for Molecular Science
Institute of Chemistry
Chinese Academy of Sciences
Beijing 100190, P. R. China
Prof. Z. Shuai
Department of Chemistry
Tsinghua University
Beijing 100084, P. R. China
Prof. X. Guo
Department of Materials Science and Engineering
College of Engineering
Peking University
Beijing 100871, P. R. China
[+]Present address: Key Laboratory of Functional Polymer Materials, Ministry of Education, Synergetic Innovation Center of Chemical Science and Engineering (Tianjin), and College of Chemistry, Nankai University, Tianjin 300071, P. R. China

DOI: 10.1002/aelm.201500159

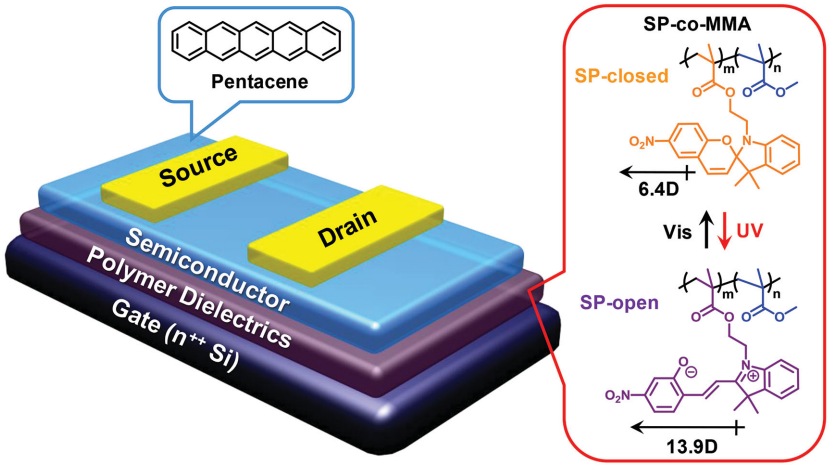

Figure 1. Schematic representation of the OFET architecture with the SP-*co*-MMA gate dielectrics. Photochromic SPs in the polymer dielectrics on the n^{++} Si substrates undergo reversible photoisomerization between SP-closed and SP-open forms, thus modulating device photocurrents.

improving device photoresponsivity (approximately three orders of magnitude). In fact, integrating photochromics into organic electronic circuits has been proven to be reliable for constructing new generations of multifunctional interfaces such as an electrode/semiconductor interface,[13] environment/semiconductor interface,[11,14] or even as a binary mixture in the active layer[15] to impart light-responsive properties into OFETs.

Figure 1 shows a standard top-contact, bottom-gate OFET device architecture on the n^{++} silicon substrates. The devices were fabricated by using a 40-nm-thick pentacene semiconductor layer on a 600-nm-thick copolymer insulator for demonstrating significant potential for incorporation into electronic circuitry. A series of photosensitive copolymers composed of SP and MMA with different SP–MMA ratios was used as the photoactive gate dielectrics. PMMA was selected as the polymer binder because it has good surface uniformity, low surface roughness, and appropriate surface energy.[16] **Table 1** shows the different monomer feed ratios used to prepare side-chain SP-*co*-MMA by atom transfer radical polymerization (ATRP). The details of the polymer synthesis are given in the Supporting Information. The molar percentages of the SP units in the copolymers were determined by the elemental analysis of nitrogen contents. Apparently, higher molar percentages of SP units are observed in the copolymers as compared to those of the SP monomer in the initial monomer feed, suggesting the higher reactivity of SP as compared to MMA in copolymerization. The weight-average molecular weights (M_w) and polydispersity index (PDI) of the resultant polymers were obtained by gel permeation chromatography (GPC, Table 1). SP-*co*-MMA-4 with the highest SP percentage (SP content: ≈32.3%) has the lowest molecular weight and the highest PDI, probably because it has poor solubility during polymerization when the SP ratio exceeds a critical value. Thus, we used SP-*co*-MMA with three different SP molar percentages of 8.9%, 13.7%, and 20.8% (labeled as SP-*co*-MMA-1, SP-*co*-MMA-2, and SP-*co*-MMA-3, respectively) as the dielectric layers to fabricate photosensitive OFETs. These SP ratios significantly exceed the saturation concentration of SPs dissolved in PMMA (≈7.0×10^2 M),[9d] which is of crucial importance to improve the photoresponsivity of the device.

Table 1. Characterization data of SP-*co*-MMA.

Polymer	Reagent ratio (SP:MMA)[a]	Product ratio (SP:MMA)[b]	SP content[b] [mol%]	M_w ($\times 10^4$)[c]	PDI[c]
SP-*co*-MMA-1	1:32	1:10.2	8.9	9.7	1.17
SP-*co*-MMA-2	1:16	1:6.3	13.7	10.7	1.18
SP-*co*-MMA-3	1:8	1:3.8	20.8	12.1	1.13
SP-*co*-MMA-4	1:4	1:2.1	32.3	6.6	1.54

[a]The molar ratio of the SP monomer in the initial monomer feed; [b]The molar ratio and percentage of SP units in the polymers determined by elemental analysis; [c]The weight-average molecular weights (M_w) and polydispersity index (PDI) of the resultant copolymers obtained from by GPC using polystyrene standards.

The maximum root-mean-square roughness obtained form tapping-mode atomic force microscopy (AFM) is less than 0.5 nm, indicating that the spin-coated copolymer gate dielectric has a smooth surface (Figure S1, Supporting Information). Figure S2 (Supporting Information) shows the UV–vis plots of the representative SP-*co*-MMA-3 copolymer film: SP units in the dielectric layers can switch back and forth between the SP-open and SP-closed forms on irradiation by UV and visible light. As obtained from the kinetic data determined by UV–vis absorption spectra, $K_{(\text{UV-spectrum})} = \approx 4.8 \pm 0.6 \times 10^{-3}$ s^{-1} and $K_{(\text{Visible-spectrum})} = \approx 1.4 \pm 0.3 \times 10^{-3}$ s^{-1} (the data in the dark not shown), which are very similar to those reported previously.[11] Notably, the photoisomerization of SP units induced by sufficient UV irradiation does not alter the surface roughness and uniformity of the copolymer films. This precludes the possibility that the changes in surface morphology induce the variance of the device conductance observed below.

After the characterization of the SP-*co*-MMA, 40 nm pentacene thin-film transistors (length: 70 μm and width: 2 mm) were fabricated on these copolymer gate insulators with a thickness of 600 nm. **Figure 2**a,b as well as Figure S3 and Table S1 (Supporting Information) summarize the saturation field-effect mobilities (μ) and capacitances (C) on different copolymer gate dielectrics. The average saturation carrier mobility (μ_{max}) of these devices is ≈0.12 cm^2 V^{-1} s^{-1}, which is higher than those of devices on SP–PMMA hybrid dielectrics (≈0.02 cm^2 V^{-1} s^{-1})[9d] and SP-monolayer-modified silicon substrates (≈0.03 cm^2 V^{-1} s^{-1}).[9c] In the subsequent analysis of the photoswitching processes, the photocurrent jumps of the transistors induced by UV and visible irradiation is controlled to the same value. Therefore, the negligible current jumps of the devices during switching between UV and visible irradiation were recorded.

Figure 2a,b also show the transfer and output curves of the representative photoresponsive devices with the SP-*co*-MMA-3

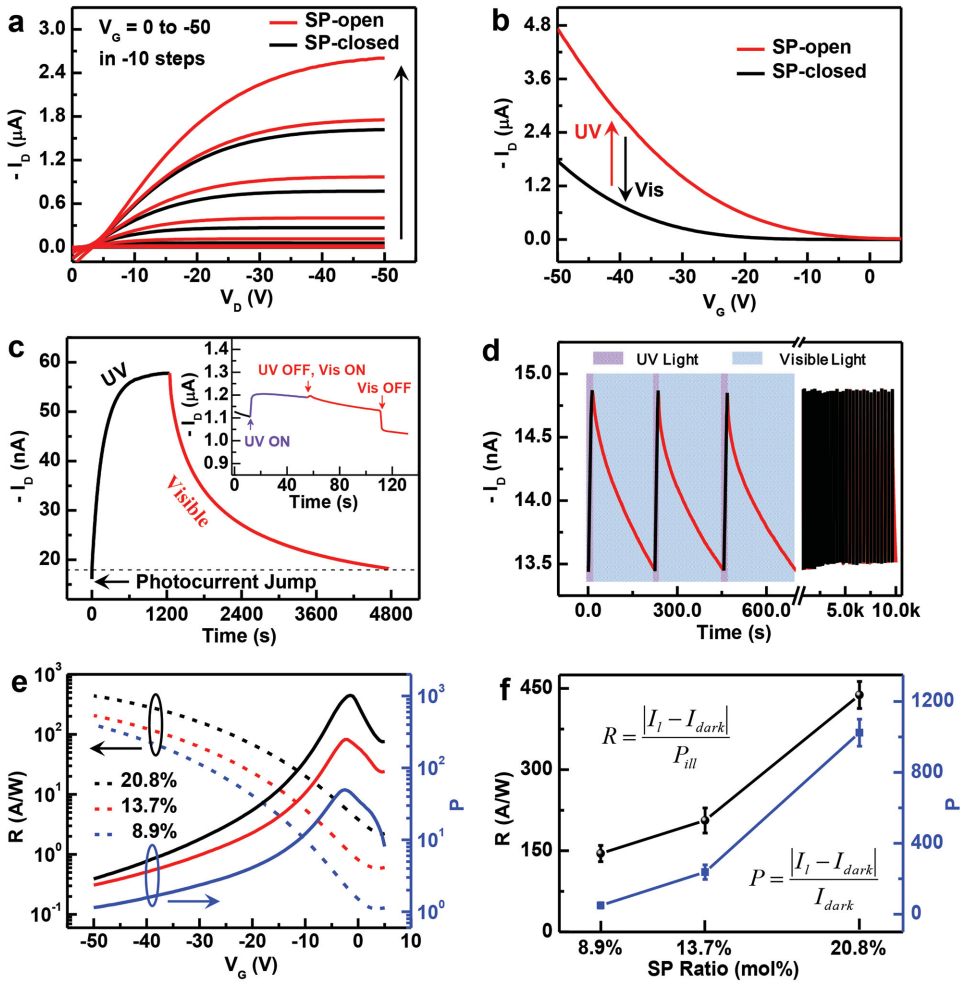

Figure 2. Photoresponsive characteristics of pentacene OFETs with SP-*co*-MMA gate dielectrics. a) Output and b) transfer properties of a SP-*co*-MMA-3 device before and after UV irradiation. $V_D = -50$ V. c) Temporal evolution of I_D with one complete cycle, $V_D = -30$ V and $V_G = -15$ V. The inset shows the time evolution of I_D for a control device with PMMA dielectrics, which does not contain SP units, under UV (365 nm) and visible ($\lambda > 520$ nm) irradiation. $V_D = -30$ V and $V_G = -15$ V. d) Time evolution of I_D for the same device over a period of ≈3 h with the first three cycles expanded for clarity, indicating reversible photoswitching modulation under UV and visible irradiation. $V_D = -30$ V and $V_G = -15$ V. e) Responsivity (R) and photosensitivity (P) values with the evolution of V_G for SP-*co*-MMA devices with three different molar percentages of SP units. $V_D = -50$ V and the irradiance power is 7.4 μmW cm^{-2}. f) Both R and P values increase with increasing molar percentages of SP units (10 devices for each SP ratio).

gate dielectrics; when exposed to UV and visible light, the drain current (I_D) can be reversibly modulated. Figure 2c shows the temporal evolution of the current–voltage curves for one complete switching cycle under UV and visible irradiation. After UV light irradiation for 1200 s, I_D clearly increases rapidly to a saturation value. Meanwhile, after another ≈3600 s of visible light irradiation, the I_D of the reverse process decreased, and the high-conductance state was converted to its original low-conductance state. The current–voltage curves of each process can be fitted with a single exponential. The kinetic results determined by current measurements indicated that $K_{(\text{UV-current})} = \approx 5.6 \pm 0.6 \times 10^{-3}$ s^{-1} and $K_{(\text{Visible-current})} = \approx 1.7 \pm 0.3 \times 10^{-3}$ s^{-1}, which are in good agreement with the kinetic results calculated from spectral measurements. The similarity between the reversible photoswitching of the conductance of the SP-functionalized devices and the reversible photoisomerization of SPs in the copolymer thin films suggests that the photoisomerization of SPs is responsible for the modulations of OFET characteristics. We fabricated a control device on the PMMA polymer dielectrics, which does not contain SP units to rule out potential artifacts (Figure 2c inset). Regardless of whether the control device is irradiated by UV or visible light, it only exhibits a slight current jump and a slow decrease of I_D. The overall rate constants ($K_{(\text{UV-current})} = K_{(\text{Visible-current})} = \approx 2.3 \pm 0.1 \times 10^{-4}$ s^{-1}) calculated from the trace in the Figure 2c inset are one order of magnitude smaller than those obtained from the SP copolymer-functionalized devices. The kinetic data obtained from Figure 2c indicated that the percentage conversion (x_e) of SPs from the SP-closed to SP-open form at the photostationary state is ≈74.3% (see the Supporting Information). At short irradiation times, these devices exhibit a long-term operational stability in a reversible manner. Figure 2d shows that the devices exhibit long-term operational stability (>50 switching cycles) without obvious degradation at

room temperature and ambient atmosphere after operation over a period of ≈3 h.

As compared to normal OFETs, photosensitive devices have two important criteria, responsivity (R) (expressed in A W^{-1}) and current change ratio (P), which determine the efficacy of the device. We calculated these parameters from the current changes in Figure 2 by using a previously defined model:[7c]

$$R = \frac{I_{light}}{P_{ill}} = \frac{|I_l - I_{dark}|}{P_{ill}} = \frac{|I_1 - I_{dark}|}{I_{ill} L W};$$
$$P = \frac{signal}{noise} = \frac{I_{light}}{I_{dark}} = \frac{|I_1 - I_{dark}|}{I_{dark}}$$

where I_{light} is the drain current induced by light, I_l is the drain current under illumination, I_{dark} is the drain current in the dark, P_{ill} is the incident illumination power on the device channel, I_{ill} is the light power intensity, L is the channel length, and W is the channel width. The R value reveals the extent of transformation of optical energy to electrical current, while the P value indicates the signal-to-noise ratio. Photoresponsivity is clearly dependent on bias. Figure 2e,f show the responsivity data of the working devices with different SP-*co*-MMA dielectrics (SP ratios of 8.9%, 13.7%, 20.8%) with the evolution of V_G (V_D = −50 V). As expected, both R and P values increase with increasing molar percentages of SP units. For devices with an SP molar percentage of 20.8%, the best data obtained are R = ≈4.5 × 10^2 A W^{-1} and P = ≈1.0 × 10^3 using light with a very low effective I_{ill} of 7.4 μW cm^{-2}. These values are significantly greater than those obtained from SP–PMMA hybrid devices (R: ≈2 A W^{-1}; P: ≈3.0)[9d] and most other organic phototransistors;[7c] furthermore, these values are comparable to those obtained from amorphous silicon-based devices (R = 300 A W^{-1} and P = 1000).[17] Considering the low photoresponsivity of pentacene itself (≈10 A W^{-1}), we conclude that the high photoresponsivity of our functional devices predominantly originates from the photoisomerization of SP units in SP-*co*-MMA (>95% contribution), in stark contrast to other small-molecule-based phototransistors where the P values mainly originated from the photoresponses of the semiconductor itself.[7] These results demonstrate the efficiency of our strategy for constructing organic phototransistors with high responsivity by developing new types of photoactive polymer gate dielectrics based on photochromic molecules, regardless of the R and P values of organic semiconductors themselves.

It is essential to investigate the mechanism as to why the photosensitivity of the SP-*co*-MMA devices in this study is significantly higher than that of SP hybrid devices. In our previous study, we demonstrated that the changes in the capacitance of the SP–PMMA hybrid dielectrics, which are blends of PMMA and SP with various thickness (150–1200 nm), are responsible for the modulation of the drain current in the devices.[9d] Similarly, in this study of SP-*co*-MMA dielectrics, we have reason to believe that the reversible modulation of the capacitance of copolymer dielectrics, which is induced by the photoisomerization of SPs, is also one of the reasons for the high photoresponsitivity. Molecular dynamics (MD) simulations can aid in the calculation of the static dielectric constants of SP-*co*-MMA by utilizing the fluctuation of the dipole moment. Hence, MD calculations were performed with the Materials Studio software to verify this mechanism. The computational procedure of MD simulations and evaluation of dielectric constants are provided in the Supporting Information. Based on the calculations, the converged permittivity of the SP-*co*-MMA-3 with SP-closed is ≈2.75 (**Figure 3**a). As compared to this value, the permittivity of the copolymers with SP-open is ≈3.45, which is ≈25% greater than that with SP-closed. This simulation result demonstrated that the photoisomerization of SPs induces a significant change in the permittivity of the copolymers caused by molecular dipoles.

To experimentally prove this theoretical prediction, we measured the capacitance of SP-*co*-MMAs using a sandwich device architecture. Figure 3b,c show the temporal evolution of the capacitance data of the SP-*co*-MMA-3 dielectrics with a film thickness of 600 nm. On exposure to UV light, a gradual transition from low- to high-capacitance states is remarkably observed. After the devices were exposed to UV light for ≈720 s, the capacitance gradually increases to saturation. Similarly, under visible irradiation, the recovery process is realized. As shown in Figure 3c, after another ≈24 min of exposure to visible light, the high-capacitance state slowly converted back to the original low-capacitance state, completing a full switching cycle. Notably, the devices exhibit reversible photoswitching processes. The capacitance of the same device was measured at a frequency of 1 MHz. The four complete switching cycles are shown in Figure 3d. Based on the capacitance curves in Figure 3d, the kinetic rate constants are calculated as $K_{(UV\text{-}capacitance)}$ = ≈5.5 ± 0.8 × 10^{-3} s^{-1} and $K_{(Visible\text{-}current)}$ = ≈1.6 ± 0.2 × 10^{-3} s^{-1}. Remarkably, the kinetic data obtained from the observed capacitance photoswitching in SP-*co*-MMA are nearly the same as those obtained from the conductance in the devices (Figure 2c) and UV–vis absorption studies (Figure S2, Supporting Information). As reported previously, regardless of irradiation by visible or UV light, the changes in the capacitance of the control PMMA dielectrics are nearly negligible.[9d] Therefore, these results indicate that the photoswitching of the capacitance in SP-functionalized transistors originates from the photoisomerization of SP units. The photoisomerization of SPs induces a significant alteration in the dipole moment, which would initiate a collective variation in the dielectric constant of the copolymer, thus leading to the reversible photomodulation of the capacitance of the polymer dielectrics. The gate dielectric with a higher capacitance value can store more charges at the semiconductor/dielectric interface at similar voltages, leading to an increase of the carrier density, and consequently, drain current, in the devices.[7a] **Figure 4** shows the switching mechanism based on conformation-induced capacitive coupling before and after UV irradiation. The percentage change in the capacitance predicted by theory (≈25%) is higher than that obtained from actual experiments (≈10%), probably caused by the incomplete conversion of SP units under illumination (≈74.3% from SP-closed to SP-open) and the unoptimized operation conditions (Table S1, Supporting Information).

As compared to previous studies, in this study, the SP content in the SP-*co*-MMA dielectrics is more than that in SP hybrid devices; thus, the photoresponsivity of the SP copolymer device is greater than that of the SP hybrid devices. However,

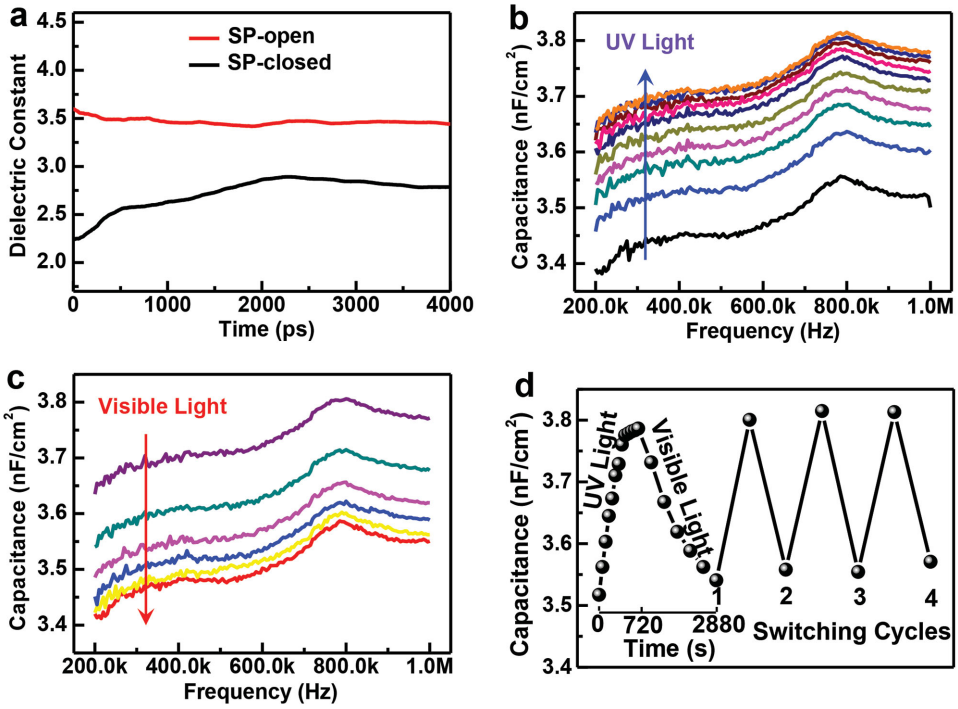

Figure 3. Demonstration of capacitance modulation. a) Simulated static dielectric constants with the temporal evolution for an SP-*co*-MMA-3 system with SP-closed (black) and SP-open (red) using a configuration average scheme. b,c) Gradual transitions of the capacitances of SP-*co*-MMA-3 copolymer dielectrics between low- and high-capacitance states when the curves were recorded every 60 s under UV light irradiation (b) and every 360 s under visible light irradiation (c). The film thickness is 600 nm. d) Four complete switching cycles of the capacitance which were measured at the data at the frequency 1 MHz.

even by increasing capacitance, induced by the increase of the SP content, the significant increase in the *R* and *P* values could not be completely explained. As a result, the photoswitching mechanism has to be investigated in detail. Photogenerated carriers (or charges) in semiconductors are well known to contribute significantly to device photocurrents.[7a] Generally, it is difficult to separate photogenerated excitons in organic semiconductors, which are a bound electron-hole pair with a strong exciton binding energy, to yield free charges. As a result, the free charges resulting from the separation of photogenerated excitons assisted by external forces can provide additional photocurrent.[18] As reported in our previous

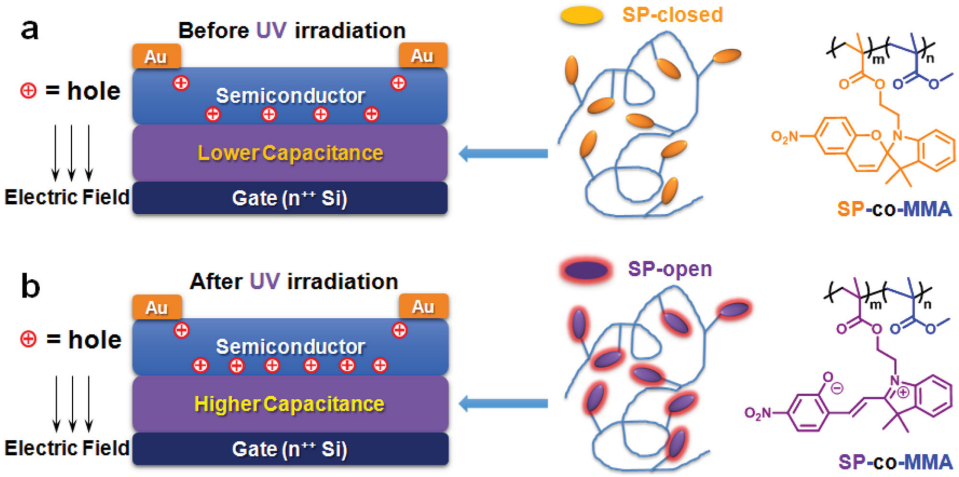

Figure 4. Proposed model of a conformation-induced capacitive coupling mechanism. a) Before UV irradiation, the initial relatively low capacitance value induces the formation of pristine charges at the dielectric/semiconductor interface. b) After UV irradiation, the higher capacitance can produce more charge carriers at the dielectric/semiconductor interface under the same condition, thus leading to an increase of the carrier density, and consequently, the drain current, in the devices.

study, when charge-separated SP-open is assembled on the surface of single-walled carbon nanotubes[12e] or blended with poly(3-hexylthiophene-2,5-diyl) (P3HT) semiconductors,[15c] it can introduce scattering sites for the carriers by creating localized dipole fields around the conductive channel. Then, these sites facilitate the separation of the photogenerated excitions. Thus, in this study, with the increase of the SP ratio in dielectrics, the SP units at the dielectric/semiconductor interface play a more important role. Therefore, we conclude that the charge-separated SP-open units in the SP-*co*-MMA copolymer dielectrics probably behave similar to electron traps at the dielectric/semiconductor interface and keep the hole carriers in the channel, thus causing an increase in the photocurrent. On irradiation by UV light, the zwitterion of SP-open at the dielectric/semiconductor interface enhances charge separation efficiency and increases hole carrier density, thereby resulting in a large threshold shift and a higher current. In contrast, on irradiation by visible light, SP-closed cannot capture electrons, and the photogenerated excitons that have not arrived at the conducting channel will be recombined, thus decreasing the current. This increase in the current is demonstrated by the fact that a dramatic V_T shift from ≈–28.6 to ≈–7.1 V is observed on irradiation by UV light (Figure S3 and Table S1, Supporting Information), and the V_T shift could be restored to its original value under additional irradiation by visible light.[9c] This threshold voltage shift is attributed to the charged nature of the SP-open zwitterion, which is capable of trapping the photostimulated electrons, thus increasing the hole density at the dielectric/semiconductor interface. However, the manner in which the zwitterions of SP-open quench the electron carriers in the channel is still unclear, necessitating further investigation.

To further understand the underlying physical mechanism of electron trapping, we used an interfacial space charge layer model to provide the quantitative explanation of the threshold voltage shift.[19] This charge layer at the dielectric/semiconductor interface originates from the photoinduced charge traps of SP units close to the interface. These traps produce an effective gate voltage (V_{eff}) that results in a shift of the threshold voltage (ΔV_{th}). In this model, V_{eff} is given by

$$V_{eff} = V_G + \frac{\sigma_{sp}}{C_{sp}}$$

where σ_{sp} is the surface density of the photoinduced charges of SP units, V_G is the gate voltage and C_{sp} is the capacitance of SP-*co*-MMA copolymer dielectrics. This equation implies that V_G is shifted by an additional voltage drop σ_{sp}/C_{sp}. The term of σ_{sp}/C_{sp} is simply a consequence of the continuity requirement for the displacement field across the interface (Gauss' law). When $V_G = 0$ V, we can obtain ΔV_{th} from the value of V_{eff}. The value of σ_{sp} is calculated to be $\approx 2.78 \times 10^{12}$ cm^{-2}, which can be estimated by the areal density of SP units in copolymer dielectric (The calculation details are given in the Supporting Information). The value of C_{sp} is 3.85 nF cm^{-2} (Figure 3b and Table S1, Supporting Information). Therefore, the ΔV_{th} is calculated to be ≈78.5 V, which is in the same order with the experimental value (21.5 V). This result demonstrates that the interfacial space charge layer can, indeed, shift the threshold voltage by several ten volts, which significantly contributes to the device current. The minor deviation of this simple ΔV_{th} calculation from the experimental data is probably caused by the insufficient accuracy of the σ_{sp} value and the rechargeable trap states as well as a carrier-density dependence of the mobility in the calculation. In some cases, the shift of V_{th} also results from the dipole layer at the dielectric/semiconductor interface. However, to explain the shift in V_{th} up to 21.5 V observed in the devices, one has to assume a dipole moment that exceeds 21.9 D (see the Supporting Information). Considering such a high value of a dipole moment, we conclude that the small change in the dipole moment of SP units has the negligible effect on the shift of V_{th}, but has the obvious effect on the dielectric capacitance as demonstrated above. Therefore, SP photoisomerization can produce an interfacial charge layer, which leads to the threshold voltage shift, and simultaneously increase the dielectric capacitance. As a result, it is reasonable that the 1000-fold increase in device photoresponsivity results form the synergistic modulation of the dielectric capacitance and charge trapping effect.

In addition, another possible switching mechanism is the variation in the surface uniformity and roughness of the pentacene layer. To preclude the possibility, the morphology of the copolymer films was characterized by AFM as demonstrated previously. No obvious morphological changes are observed for the SP-*co*-MMA dielectric layer before and after UV irradiation (Figure S1, Supporting Information). Consequently, it is reasonable that by using SP-*co*-MMA dielectrics, an improvement in photoresponsivity of nearly three orders of magnitude is observed by synergistic effects of the confirmed capacitive coupling and charge separation induced by conformational changes at the dielectric/semiconductor interface.[19] Notably, all conformational changes occurring within the dielectric layer are driven by the most convenient and non-invasive tool of light without any damage to the organic semiconductors, thus demonstrating the operational stability of the functioning devices.

In summary, we demonstrated here an efficient approach for preparing functional OFETs with high responsivity, which are capable of photomodulating the carrier density in the conductive channel by using SP-*co*-MMA as the photoactive gate dielectrics. SP photoisomerization initiates reversible modulation in the dipole moment of SPs, thereby resulting in different capacitance values of polymer dielectrics, which induce distinct capacitive coupling at the semiconductor/dielectric interface. On the other hand, the formation of the photogenerated SP-open zwitterions produce scattering sites and quench the photoexcited electrons, thus facilitating separation–transport of hole carriers in the conductive channel. Because of the synergistic effects of both switching mechanisms, the threshold voltages can be tuned; this tuning modulates the channel conductance in a noninvasive manner, thereby leading to a new type of low-cost OFET-based photodetectors with high photosensitivity (R: $\approx 4.5 \times 10^2$ A W^{-1}; P: $\approx 1.0 \times 10^3$). Therefore, these results will help in the understanding of interfacial phenomena in greater detail and offer fresh insights into developing new strategies

for building multifunctional OFETs and ultrasensitive sensors by interface engineering. In addition to their potential use as sensors and detectors, our approach of incorporating molecular functionalities into electrical circuits promises the design and fabrication of a new generation of multifunctional interfaces, materials, and devices.

Supporting Information

Supporting Information is available from the Wiley Online Library or from the author.

Acknowledgements

The authors thank Dr. Linjun Wang, Ziyuan Song, and Prof. Zichen Li for insightful discussions. This work was supported by the 973 Project (2012CB921404), National Natural Science Foundations of China (21225311, 91333102, 21373014 and 21404060), and Natural Science Foundations of Tianjin (14JCQNJC03800).

Received: May 13, 2015
Revised: July 12, 2015
Published online: August 6, 2015

[1] a) C. D. Dimitrakopoulos, P. R. L. Malenfant, *Adv. Mater.* **2002**, *14*, 99; b) J. E. Anthony, *Chem. Rev.* **2006**, *106*, 5028; c) A. R. Murphy, J. M. J. Fréchet, *Chem. Rev.* **2007**, *107*, 1066; d) H. Sirringhaus, *Adv. Mater.* **2014**, *26*, 1319; e) C. Wang, H. Dong, W. Hu, Y. Liu, D. Zhu, *Chem. Rev.* **2011**, *112*, 2208.

[2] a) Y. Yuan, G. Giri, A. L. Ayzner, A. P. Zoombelt, S. C. B. Mannsfeld, J. Chen, D. Nordlund, M. F. Toney, J. Huang, Z. Bao, *Nat. Commun.* **2014**, *5*, 35; b) H. Minemawari, T. Yamada, H. Matsui, J. Y. Tsutsumi, S. Haas, R. Chiba, R. Kumai, T. Hasegawa, *Nature* **2011**, *475*, 364; c) A. Y. Amin, A. Khassanov, K. Reuter, T. Meyer-Friedrichsen, M. Halik, *J. Am. Chem. Soc.* **2012**, *134*, 16548; d) W. Xie, K. Willa, Y. Wu, R. Häusermann, K. Takimiya, B. Batlogg, C. D. Frisbie, *Adv. Mater.* **2013**, *25*, 3478; e) H.-R. Tseng, H. Phan, C. Luo, M. Wang, L. A. Perez, S. N. Patel, L. Ying, E. J. Kramer, T.-Q. Nguyen, G. C. Bazan, A. J. Heeger, *Adv. Mater.* **2014**, *26*, 2993; f) G. Kim, S.-J. Kang, G. K. Dutta, Y.-K. Han, T. J. Shin, Y.-Y. Noh, C. Yang, *J. Am. Chem. Soc.* **2014**, *136*, 9477; g) X. Liu, Y. Guo, Y. Ma, H. Chen, Z. Mao, H. Wang, G. Yu, Y. Liu, *Adv. Mater.* **2014**, *26*, 3631; h) Y. Wu, B. Su, L. Jiang, A. J. Heeger, *Adv. Mater.* **2013**, *25*, 6526; i) K. Takimiya, S. Shinamura, I. Osaka, E. Miyazaki, *Adv. Mater.* **2011**, *23*, 4347.

[3] a) T. Sekitani, T. Yokota, U. Zschieschang, H. Klauk, S. Bauer, K. Takeuchi, M. Takamiya, T. Sakurai, T. Someya, *Science* **2009**, *326*, 1516; b) S.-T. Han, Y. Zhou, V. A. L. Roy, *Adv. Mater.* **2013**, *25*, 5425; c) R. C. G. Naber, K. Asadi, P. W. M. Blom, D. M. de Leeuw, B. de Boer, *Adv. Mater.* **2010**, *22*, 933; d) W. L. Leong, N. Mathews, B. Tan, S. Vaidyanathan, F. Dotz, S. Mhaisalkar, *J. Mater. Chem.* **2011**, *21*, 5203.

[4] a) Y. Guo, C. Du, G. Yu, C.-a. Di, S. Jiang, H. Xi, J. Zheng, S. Yan, C. Yu, W. Hu, Y. Liu, *Adv. Funct. Mater.* **2010**, *20*, 1019; b) S. Liu, Z. Wei, Y. Cao, L. Gan, Z. Wang, W. Xu, X. Guo, D. Zhu, *Chem. Sci.* **2011**, *2*, 796; c) X. Guo, S. Xiao, M. Myers, Q. Miao, M. L. Steigerwald, C. Nuckolls, *Proc. Natl. Acad. Sci. USA* **2009**, *106*, 691; d) T. P. I. Saragi, T. Spehr, A. Siebert, T. Fuhrmann-Lieker, J. Salbeck, *Chem. Rev.* **2007**, *107*, 1011; e) S. Liu, X. Guo, *Acta Chim. Sinica* **2013**, *71*, 478.

[5] a) J. Zaumseil, R. H. Friend, H. Sirringhaus, *Nat. Mater.* **2006**, *5*, 69; b) H. Nakanotani, M. Saito, H. Nakamura, C. Adachi, *Appl. Phys. Lett.* **2009**, *95*, 103307; c) S. Z. Bisri, T. Takenobu, Y. Yomogida, H. Shimotani, T. Yamao, S. Hotta, Y. Iwasa, *Adv. Funct. Mater.* **2009**, *19*, 1728.

[6] a) T. Someya, T. Sekitani, S. Iba, Y. Kato, H. Kawaguchi, T. Sakurai, *Proc. Natl. Acad. Sci. USA* **2004**, *101*, 9966; b) X. Guo, M. Myers, S. Xiao, M. Lefenfeld, R. Steiner, G. S. Tulevski, J. Tang, J. Baumert, F. Leibfarth, J. T. Yardley, M. L. Steigerwald, P. Kim, C. Nuckolls, *Proc. Natl. Acad. Sci. USA* **2006**, *103*, 11452; c) M. E. Roberts, S. C. B. Mannsfeld, N. Queraltó, C. Reese, J. Locklin, W. Knoll, Z. Bao, *Proc. Natl. Acad. Sci. USA* **2008**, *105*, 12134; d) P. Stoliar, E. Bystrenova, S. D. Quiroga, P. Annibale, M. Facchini, M. Spijkman, S. Setayesh, D. de Leeuw, F. Biscarini, *Biosens. Bioelectron.* **2009**, *24*, 2935; e) G. Schwartz, B. C. K. Tee, J. Mei, A. L. Appleton, D. H. Kim, H. Wang, Z. Bao, *Nat. Commun.* **2013**, *4*, 1859; f) L. Torsi, G. M. Farinola, F. Marinelli, M. C. Tanese, O. H. Omar, L. Valli, F. Babudri, F. Palmisano, P. G. Zambonin, F. Naso, *Nat. Mater.* **2008**, *7*, 412; g) S. C. B. Mannsfeld, B. C. K. Tee, R. M. Stoltenberg, C. V. H. H. Chen, S. Barman, B. V. O. Muir, A. N. Sokolov, C. Reese, Z. Bao, *Nat. Mater.* **2010**, *9*, 859.

[7] a) K.-J. Baeg, M. Binda, D. Natali, M. Caironi, Y.-Y. Noh, *Adv. Mater.* **2013**, *25*, 4267; b) E. Orgiu, P. Samorì, *Adv. Mater.* **2014**, *26*, 1827; c) Y. Guo, G. Yu, Y. Liu, *Adv. Mater.* **2010**, *22*, 4427; d) Y. Cao, M. L. Steigerwald, C. Nuckolls, X. Guo, *Adv. Mater.* **2010**, *22*, 20; e) M. Magliulo, K. Manoli, E. Macchia, G. Palazzo, L. Torsi, *Adv. Mater.* **2014**, DOI: 10.1002/adma.201403477; f) S. Nau, C. Wolf, S. Sax, E. J. W. List-Kratochvil, *Adv. Mater.* **2015**, *27*, 1048; g) C. Liao, M. Zhang, M. Y. Yao, T. Hua, L. Li, F. Yan, *Adv. Mater.* **2014**, DOI: 10.1002/adma.201402625; h) Y.-Y. Noh, D.-Y. Kim, *Solid-State Electron.* **2007**, *51*, 1052.

[8] a) C.-A. Di, Y. Liu, G. Yu, D. Zhu, *Acc. Chem. Res.* **2009**, *42*, 1573; b) C. Jia, X. Guo, *Chem. Soc. Rev.* **2013**, *42*, 5642.

[9] a) S. Kobayashi, T. Nishikawa, T. Takenobu, S. Mori, T. Shimoda, T. Mitani, H. Shimotani, N. Yoshimoto, S. Ogawa, Y. Iwasa, *Nat. Mater.* **2004**, *3*, 317; b) Q. Shen, Y. Cao, S. Liu, L. Gan, J. Li, Z. Wang, J. Hui, X. Guo, D. Xu, Z. Liu, *J. Phys. Chem. Lett.* **2010**, *1*, 1269; c) H. Zhang, X. Guo, J. Hui, S. Hu, W. Xu, D. Zhu, *Nano Lett.* **2011**, *11*, 4939; d) Q. Shen, L. Wang, S. Liu, Y. Cao, L. Gan, X. Guo, M. L. Steigerwald, Z. Shuai, Z. Liu, C. Nuckolls, *Adv. Mater.* **2010**, *22*, 3282; e) U. Kraft, M. Sejfi , M. J. Kang, K. Takimiya, T. Zaki, F. Letzkus, J. N. Burghartz, E. Weber, H. Klauk, *Adv. Mater.* **2015**, *27*, 207; f) P. Lutsyk, K. Janus, J. Sworakowski, G. Generali, R. Capelli, M. Muccini, *J. Phys. Chem. C* **2011**, *115*, 3106; g) C. S. Smithson, Y. Wu, T. Wigglesworth, S. Zhu, *Adv. Mater.* **2015**, *27*, 228.

[10] a) G. Berkovic, V. Krongauz, V. Weiss, *Chem. Rev.* **2000**, *100*, 1741; b) V. I. Minkin, *Chem. Rev.* **2004**, *104*, 2751.

[11] a) Q. Shen, Y. Cao, S. Liu, M. L. Steigerwald, X. Guo, *J. Phys. Chem. C* **2009**, *113*, 10807; b) B. C. Bunker, B. I. Kim, J. E. Houston, R. Rosario, A. A. Garcia, M. Hayes, D. Gust, S. T. Picraux, *Nano Lett.* **2003**, *3*, 1723.

[12] a) B. I. Ipe, S. Mahima, K. G. Thomas, *J. Am. Chem. Soc.* **2003**, *125*, 7174; b) I. Vlassiouk, C.-D. Park, S. A. Vail, D. Gust, S. Smirnov, *Nano Lett.* **2006**, *6*, 1013; c) M. Lion-Dagan, E. Katz, I. Willner, *J. Am. Chem. Soc.* **1994**, *116*, 7913; d) G. Jiang, Y. Song, X. Guo, D. Zhang, D. Zhu, *Adv. Mater.* **2008**, *20*, 2888; e) X. Guo, L. Huang, S. O'Brien, P. Kim, C. Nuckolls, *J. Am. Chem. Soc.* **2005**, *127*, 15045; f) X. Guo, D. Zhang, G. Yu, M. Wan, J. Li, Y. Liu, D. Zhu, *Adv. Mater.* **2004**, *16*, 636; g) C. P. Collier, B. Ma, E. W. Wong, J. R. Heath, F. Wudl, *ChemPhysChem* **2002**, *3*, 458.

[13] N. Crivillers, E. Orgiu, F. Reinders, M. Mayor, P. Samorì, *Adv. Mater.* **2011**, *23*, 1447.

[14] Y. Ishiguro, R. Hayakawa, T. Yasuda, T. Chikyow, Y. Wakayama, *ACS Appl. Mater. Interfaces* **2013**, *5*, 9726.
[15] a) C. Raimondo, N. Crivillers, F. Reinders, F. Sander, M. Mayor, P. Samorì, *Proc. Natl. Acad. Sci. USA* **2012**, *109*, 12375; b) E. Orgiu, N. Crivillers, M. Herder, L. Grubert, M. Pätzel, J. Frisch, E. Pavlica, D. T. Duong, G. Bratina, A. Salleo, N. Koch, S. Hecht, P. Samorì, *Nat. Chem.* **2012**, *4*, 675; c) Y. Li, H. Zhang, C. Qi, X. Guo, *J. Mater. Chem.* **2012**, *22*, 4261; d) Y. Ishiguro, R. Hayakawa, T. Chikyow, Y. Wakayama, *J. Mater. Chem. C* **2013**, *1*, 3012; e) R. Hayakawa, K. Higashiguchi, K. Matsuda, T. Chikyow, Y. Wakayama, *ACS Appl. Mater. Interfaces* **2013**, *5*, 3625.
[16] S. Gross, D. Camozzo, V. Di Noto, L. Armelao, E. Tondello, *Eur. Polym. J.* **2007**, *43*, 673.
[17] Y. Kaneko, N. Koike, K. Tsutsui, T. Tsukada, *Appl. Phys. Lett.* **1990**, *56*, 650.
[18] Z. Jia, L. Banu, I. Kymissis, *IEEE Trans. Electron. Devices* **2010**, *57*, 380.
[19] S. K. Possanner, K. Zojer, P. Pacher, E. Zojer, F. Schürrer, *Adv. Funct. Mater.* **2009**, *19*, 958.